Quantum fluctuations and unusual critical exponents in a quantum Rabi triangle

Xiao Qin and Yu-Yu Zhang*

Department of Physics, Chongqing Key Laboratory for Strongly Coupled Physics, Chongqing University, Chongqing 401330, China

(Received 28 February 2024; accepted 9 July 2024; published 25 July 2024)

The quantum fluctuations of a quantum Rabi triangle are investigated using an analytical method that goes beyond mean-field theory. An artificial magnetic field applied in three cavities leads to the breaking of time-reversal symmetry, which is evident in the directional transfer of photons. In contrast to previous studies, we focus on the scaling exponents of quantum fluctuations of the local photon number and the position variance near the critical point. Specifically, the fluctuations of photons do not diverge as the coupling strength approaches the critical value from below for the chiral superradiant phase transition. Attributing to geometric frustration, two distinct scaling laws arise for the frustrated cavity and the remaining cavities. Specifically, in the frustrated cavity, the scaling exponent in the chiral superradiant phase differs from that without an artificial magnetic field for the frustrated antiferromagnetic superradiant phase. The unusual scaling exponents indicate distinct universality classes in contrast to the single-cavity Rabi one. We suggest that accurate critical exponents in few-body systems are useful for identifying exotic quantum phase transitions in light-matter coupling systems.

DOI: 10.1103/PhysRevA.110.013713

I. INTRODUCTION

The interaction between light and matter has brought forth a new class of quantum many-body systems in understanding strongly correlated systems and the quantum phase transition [1–4]. The effect of quantum fluctuations driving the quantum phase transitions is especially pronounced in characterizing singularity and universality classes by universal scaling laws [5–8]. A superradiant phase transition (SPT) is a remarkable phenomenon in the Dicke mode [9–13], which describes an ensemble of two-level atoms interacting with a quantized single-mode cavity. Such a SPT has been found in the quantum Rabi model of a single-atom system in the infinite-frequency limit [14–19], which has the same critical exponents as the Dicke model [12–14]. A few-body system of light-atom interactions sheds new light on the quantum simulation of quantum phase transitions because of its high control and tunability.

Recently, much effort has been devoted to imposing an artificial magnetic field on neutral atoms and photons [20], which have brought forth remarkable phenomena, such as chiral edge currents in atoms [21,22], chiral ground-state currents of interacting photons [23], and fractional quantum Hall physics in the Jaynes-Cummings Hubbard lattice [24,25]. In the presence of an artificial magnetic field, unusual superradiant phases have been found in the generalized Rabi and Dicke systems, including chiral superradiant phases in a quantum Rabi ring [26,27] and anomalous superradiant phases in a Dicke lattice model [28]. Such exotic SPTs exhibit unusual scaling behaviors compared to the conventional SPT in the Dicke model. In addition to the artificial magnetic field, geometric frustration has been proved to induce counterintuitive critical phenomena. Different critical exponents of the excitation energy have been found on the two sides of phase transitions in the Rabi triangle [27] and in the Dicke trimer [28,29], which are associated with frustrated geometry. However, there appear to be no clear scaling exponents of quantum fluctuations near the critical value. Since there is a challenge of an accurate solution beyond a mean-field approach for the Rabi and Dicke lattices including interactions between cavities.

In this paper, we perform an analytical solution beyond the mean-field approximation for the quantum Rabi triangle with an artificial magnetic field. In contrast to previous studies, we present an analytical expression of quantum fluctuations and obtain accurate scaling exponents near the critical point. In the chiral superradiant phase (CSP), the frustrated cavity has different photon numbers compared to the other two. Its corresponding quantum fluctuation of the photons diverges with an anomalous critical exponent, which is distinguished from the conventional exponent of the remaining cavities. Strikingly, it is different from the scaling exponent of the frustrated cavity in the frustrated antiferromagnetic superradiant phase (FASP) in the absence of an artificial magnetic field. It demonstrates that the artifical magnetic field and geometric frustration play a different role in the frustrated cavity. Thus, the scaling behavior of quantum fluctuations falls into two classes, one for the frustrated cavity and the other for the remaining cavities. Moreover, the scaling behavior below and above the transition point is different due to geometric frustration. However, the scaling exponents are equal to each other on the two sides of the transition of the ferromagnetic superradiant phase (FSP), which are the same as those in the Dicke model.

The rest of this paper is organized as follows. In Sec. II, we introduce the Hamiltonian of the quantum Rabi triangle and the dynamics of photons with an artificial magnetic field. In Sec. III, quantum fluctuations of the mean photons and the

*Contact author: yuyuzh@cqu.edu.cn

position variance are derived in the normal phase and in the superradiant phase, respectively. Section IV gives the scaling exponents of the quantum fluctuations and excitation energies beyond the mean-field approximation. The conclusion is given in Sec. V.

II. AN ARTIFICAL MAGNETIC FIELD IN A QUANTUM TRIANGLE

The quantum Rabi triangle model describes photon hopping between neighboring cavities in $N = 3$ coupled cavities, where each cavity contains a two-level atom and is described by the quantum Rabi model. The Hamiltonian reads

$$H_{\rm QRT} = \sum_{n}^{3} H_{R,n} + \sum_{n}^{3} J(e^{i\theta} a_n^\dagger a_{n+1} + e^{-i\theta} a_n a_{n+1}^\dagger), \qquad (1)$$

where the quantum Rabi Hamiltonian of each cavity is described as $H_{R,n} = \omega a_n^\dagger a_n + g(a_n^\dagger + a_n)\sigma_n^x + \frac{\Delta}{2}\sigma_n^z$. a_n ($a_n^\dagger$) is the photon annihilation (creation) operator of the single-mode cavity with the frequency ω at cavity n, and σ_n^i are the Pauli matrices of the two-level atom at site n with the transition frequency Δ. g is the atom-cavity coupling strength. The dimensionless coupling strength is defined as $g_1 = g/\sqrt{\Delta\omega}$. The quantum Rabi model exhibits a superradiant phase transition in the infinite frequency limit [14–17], where the frequency ratio $\eta = \Delta/\omega$ approaches ∞.

The second term of the Hamiltonian $H_{\rm QRT}$ describes the hopping of photons between neighboring cavities with the hopping amplitude J and a phase θ. The nonzero hopping phase θ arises from an artificial vector potential, $A(\mathbf{r})$, which leads the photon hopping terms between nearby cavities n and m to become complex with the phase given by $\theta = \int_{\mathbf{r}_n}^{\mathbf{r}_m} A(\mathbf{r})d\mathbf{r}$. The effective magnetic flux is 3θ in three cavities, which form a closed loop. The hopping phase θ can be realized by a periodic modulation of the photon hopping strength between cavities [26]. The complex hopping amplitude leads to the breaking of the time-reversal symmetry (TRS) when $\theta \neq m\pi$ ($m \in \mathbb{Z}$).

To explore the effects of the artificial magnetic field, we study the dynamics of a photon flowing in the closed-cavity loop. At $t = 0$, a photon is prepared in the first cavity, and the two-level atom in each cavity is in the down state, giving the initial state $|\varphi(0)\rangle = |100\rangle|\downarrow\downarrow\downarrow\rangle$. Figure 1 shows the dynamics of the mean photon in each cavity depending on θ. The photon number $N_i = \langle\varphi(t)|a_i^\dagger a_i|\varphi(t)\rangle$ is initially occupied in the first cavity with $N_1 = 1$. For $\theta = 0$ in Fig. 1(a), the photons transfer symmetrically from cavity 1 to cavity 2 and cavity 3 simultaneously and then transfer back to cavity 1. There is no preferred circulation direction. Since TRS is preserved for the trivial case $\theta = 0$, the states at time t and $T - t$ satisfy $\varphi(t) = \varphi(T - t)$ with a time-evolving period T. A completely different dynamics is observed for $\theta = \pi/2$ in Fig. 1(b). The photon flows unidirectionally, first from cavity 1, to cavity 2, to cavity 3, and finally back to cavity 1. Such a chiral current direction is a signature of the breaking of TRS. Because the evolution of the state from $t = T$ backward is different compared to going forward from $t = 0$, choosing $\theta = -\pi/2$ leads to the opposite direction of the chiral photon flow in Fig. 1(c).

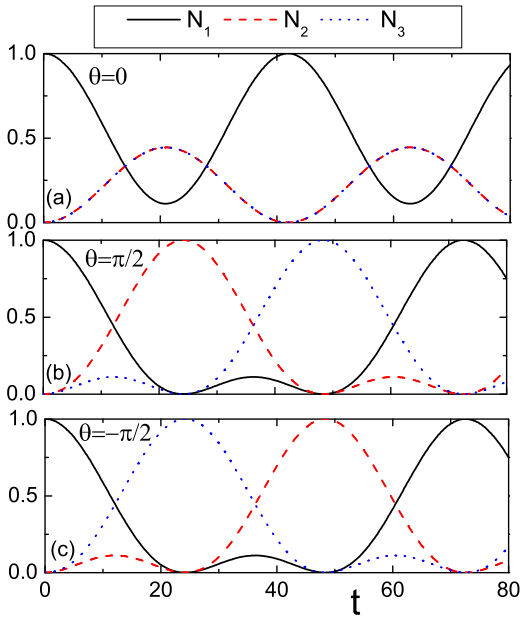

FIG. 1. Mean photon number in each cavity N_1 (black solid line), N_2 (red dashed line), and N_3 (blue dotted line) as a function of time t for three values of $\theta = 0$ (a), $\theta = \pi/2$ (b), and $\theta = -\pi/2$ (c) for the scaled coupling strength $g_1 = 0.1$. In this paper we use $\Delta/\omega = 50$ and $J/\omega = 0.05$ by choosing $\omega = 1$ as the unit for frequency.

It shows that the artificial flux θ leads to the breaking of TRS, which behaves similarly to a magnetic flux.

Besides TRS breaking induced by artificial magnetic flux, rich superradiant phase transitions have been explored depending on θ in the quantum Rabi triangle [26,27]. Unlike previous studies, we study quantum fluctuations and extract unusual critical exponents to classify the universality classes of the nontrivial phase transition beyond a mean-field approximation.

III. QUANTUM FLUCTUATIONS

Normal phase. For a weak coupling g_1, the system is in the normal phase (NP) with almost zero excitations. We perform a Schrieffer-Wolff transformation with a unitary operator $S_n = \exp[-i\sigma_n^y g_1\sqrt{\omega/\Delta}(a_n^\dagger + a_n)]$ [26]. The lower-energy Hamiltonian is obtained by projecting $H_{\rm NP}$ to the spin subspace $|\downarrow\rangle$, giving

$$H_{\rm NP}^{\downarrow} = \sum_{n=1}^{3} \left(\omega - 2\omega g_1^2\right) a_n^\dagger a_n - \omega g_1^2 \left(a_n^2 + a_n^{\dagger 2}\right) + J\sum_{\langle nn'\rangle}^{3} (e^{i\theta} a_n^\dagger a_{n'} + \text{H.c.}) + E_0, \qquad (2)$$

where the energy constant is $E_0 = 3[-\Delta/2 - \omega g_1^2 + (\omega + J)\omega^2 g_1^2/\Delta]$. The approximated Hamiltonian is valid under the conditions of $\eta \gg 1$ and $J/\omega \ll 1$.

By introducing the Fourier transformation $a_n^\dagger = \sum_q e^{inq} a_q^\dagger/\sqrt{N}$ with the quasimomentum $q = 0$ and $\pm 2\pi/3$, the transformed Hamiltonian becomes $H_{\rm NP}^{\downarrow}\sqrt{N\pi/2} = \sum_q \omega_q a_q^\dagger a_q - \omega g_1^2(a_q a_{-q} + a_q^\dagger a_{-q}^\dagger) + E_0$, with $\omega_q = \omega - 2\omega$

$g_1^2 + 2J\cos(\theta - q)$. By performing a unitary transformation $S_q = \exp[\lambda_q(a_q^\dagger a_{-q}^\dagger - a_q a_{-q})]$ with a variational squeezing parameter $\lambda_q = -\frac{1}{8}\ln\frac{\omega_q+\omega_{-q}-4\omega g_1^2}{\omega_q+\omega_{-q}+4\omega g_1^2}$, the Hamiltonian is obtained in diagonal form as $H_{\rm NP}^{\downarrow} = \sqrt{2/(N\pi)}\sum_q \varepsilon_q a_q^\dagger a_q + E_g$, with the ground-state energy E_g. The excitation spectrum is obtained as

$$\varepsilon_q^{\rm NP} = \frac{1}{2}\Big(\sqrt{\Omega_{+,q}^2 - 16\omega^2 g_1^4} + \Omega_{-,q}\Big), \tag{3}$$

with the dispersion $\Omega_{\pm,q} = \omega_q \pm \omega_{-q}$. The lowest excitation energy is associated with the quasimomentum q dependent on θ. For $\theta = 0$, the excitation energy $\varepsilon_{q=\pm 2/3}^{\rm NP}$ with $q = \pm 2\pi/3$ becomes the lowest one and decreases to 0 for g_1 approaching g_c from below in Fig. 3(a). As θ increases, the lowest energy is $\varepsilon_{q=-2/3}^{\rm NP}$ with $q = -2\pi/3$ in Fig. 3(b). Then it changes to $\varepsilon_{q=0}^{\rm NP}$ with $q = 0$ in Fig. 3(d). The vanishing of $\varepsilon_q^{\rm NP} = 0$ dependent on θ and q-momentum gives the critical scaled coupling strength $g_{1c}(q) = \frac{1}{2}\sqrt{\frac{1+4J/\omega\cos\theta\cos q+4J^2/\omega^2\cos(\theta+q)\cos(\theta-q)}{1+2J/\omega\cos\theta\cos q}}$.

The ground state in the NP is

$$|\varphi_{np}\rangle = \prod_q e^{\lambda_q(a_q^\dagger a_{-q}^\dagger - a_q a_{-q})}|0\rangle_q|\downarrow\rangle, \tag{4}$$

where $|\downarrow\rangle$ is the lowest state of the atom. The average number of photons in the ground state can be obtained as $\langle a_q^\dagger a_q\rangle_{np} = \langle\varphi_{np}|a_q^\dagger a_q|\varphi_{np}\rangle = (\cosh 4\lambda_q - 1)/2$, which describes the quantum fluctuation of photons for g_1 approaching the critical value g_{1c} from below. The local mean photon number in the nth cavity is obtained as

$$\langle a_n^\dagger a_n\rangle_{np} = \frac{1}{N}\sum_q\langle a_q^\dagger a_q\rangle_{np} = \frac{1}{2N}\sum_q\left[\frac{\Omega_{+,q}}{2\varepsilon_q - \Omega_{-,q}} - 1\right]. \tag{5}$$

The variances of the position quadrature $x_q = a_q + a_q^\dagger$ and the momentum quadrature $p_q = i(a_q^\dagger - a_q)$ are derived as $(\Delta x_q)^2 = \langle\varphi_{np}|x_q^2|\varphi_{np}\rangle - \langle\varphi_{np}|x_q|\varphi_{np}\rangle^2 = e^{4\lambda_q}$ and $(\Delta p_q)^2 = \langle p_q^2\rangle - \langle p_q\rangle^2 = e^{-4\lambda_q}$, respectively. The local variances of the position and momentum quadratures in the nth cavity are found to be

$$(\Delta x)^2 = \frac{1}{N}\sum_q(\Delta x_q)^2 = \frac{1}{N}\sum_q\frac{\Omega_{+,q} + 4\omega g_1^2}{2\varepsilon_q - \Omega_{-,q}} \tag{6}$$

and $(\Delta p_n)^2 = \frac{1}{N}\sum_q e^{-4\lambda_q}$.

This indicates that the singularity of the mean photon number $\langle a_n^\dagger a_n\rangle_{np}$, the variance of $(\Delta x_n)^2$ and $(\Delta p_n)^2$, is determined by the excitation energy ε_q and $\Omega_{-,q}$ in the denominator. Obviously, ε_q becomes 0 at the critical value g_{1c}. It is interesting to understand the divergence from $\Omega_{-,q} = 4J\sin\theta\sin q$ dependent on q and θ. In the absence of the magnetic field with $\theta = 0$ or the momentum $q = 0$, we have $\Omega_{-,q} = 0$. It leads to the singularity of quantum fluctuations of $\langle a_n^\dagger a_n\rangle_{np}$ and $(\Delta x_n)^2$ at the critical point. In contrast, for $\theta \neq 0$ and $q = \pm 2\pi/3$, it gives a nonzero value of $\Omega_{-,q}$, which results in a finite value of $\langle a_n^\dagger a_n\rangle_{\rm NP}$ and $(\Delta x_n)_{\rm NP}^2$, respectively. There appear nondivergent fluctuations in Figs. 4(b) and 5(b) for g_1 approaching g_{1c} from below.

These strikingly analytical results allow for some interesting observations at the critical value $g_{1c} = \sqrt{1 + 2\cos\theta J/\omega}/2$ for the momentum $q = 0$. As $g_1 \to g_{1c}$, the excitation energy vanishes as

$$\varepsilon_{q=0}^{\rm NP}(g_1 \to g_{1c}) \sim 8\omega g_{1c}^2(g_{1c} - g_1)^{1/2}. \tag{7}$$

This reveals that the excitation energy vanishes as $\varepsilon_{q=0}^{\rm NP} \propto (g_{1c} - g_1)^\gamma$ with the exponent $\gamma = 1/2$, which agrees well with numerical values in Fig. 3(d). In the vicinity of g_{1c}, we find that the quantum fluctuations diverge as

$$\langle a_n^\dagger a_n\rangle_{np} \sim \frac{2g_{1c}^2 - g_1^2}{\sqrt{8g_{1c}^3}}(g_{1c} - g_1)^{-1/2} \tag{8}$$

and

$$(\Delta x_n)_{np}^2 \sim \sqrt{\frac{g_{1c}}{2}}(g_{1c} - g_1)^{-1/2}. \tag{9}$$

It yields the critical exponent 1/2 for the diverging of the quantum fluctuations when g_1 approaches g_{1c} from below for the case $q = 0$, which is consistent with numerical results in Figs. 4(d) and 5(d).

Superadiant phase. As the atom-cavity coupling increases $g_1 > g_{1c}$, rich superradiant phases emerge by adjusting the flux θ [26,27]. The bosonic operator $a_n^\dagger$ (a_n) is expected to shift by a displacement transformation $D(\alpha)$ with a complex displacement $\alpha_n = A_n + iB_n$, yielding $\tilde{a}_n = D^\dagger(\alpha_n)a_n D(\alpha_n) = a_n + \alpha_n$. We consider the quantum fluctuations of the shifted bosonic operator $\tilde{a}_n$ ($\tilde{a}_n^\dagger$), which is different from the mean-field approximation. The effective low-energy Hamiltonian is obtained as follows by projecting to the spin subspace $|\downarrow\rangle$ (see Appendix A):

$$H_{\rm eff}^{\downarrow} = \sum_{n=1}^{3}\omega\tilde{a}_n^\dagger\tilde{a}_n - \frac{\lambda_n^2}{\Delta_n}(\tilde{a}_n^\dagger + \tilde{a}_n)^2 + J\tilde{a}_n^\dagger(e^{i\theta}\tilde{a}_{n+1} + e^{-i\theta}\tilde{a}_{n-1}) + E_g, \tag{10}$$

where the renormalized parameter $\Delta_n = \sqrt{\Delta^2 + 16g^2A_n^2}$, and the effective coupling strength is $\lambda_n = g\Delta/\Delta_n$. The ground-state energy is obtained as $E_g = \sum_n \omega\alpha_n^*\alpha_n + J\sum_n \alpha_n^*(e^{i\theta}\alpha_{n+1} + e^{-i\theta}\alpha_{n-1}) - \Delta_n/2$. Minimizing the energy E_g with respect to the real and imaginary parts of α_n yields

$$0 = \omega A_n - g\sin(2\gamma_n) + J[(A_{n+1} + A_{n-1})\cos\theta + (B_{n-1} - B_{n+1})\sin\theta] = 0 \tag{11}$$

and

$$0 = \omega B_n + J[\cos\theta(B_{n+1} + B_{n-1}) + \sin\theta(A_{n+1} - A_{n-1})]. \tag{12}$$

Thus, the mean value of α_n can be accurately obtained by solving the above equations.

The phase diagram is plotted in the θ-g_1 plane for the quantum Rabi triangle in Fig. 2(a). It contains three intriguing superradiant phases, which can be characterized by the order parameter α_n. First, for $\theta = 0$ and $g_1 > g_{1c}^{\rm FASP}(\pm 2\pi/3)$, α_n is real with $B_n = 0$. Geometric frustration in three cavities induces a site-dependent α_n. It is observed that one cavity ($n = 1$) always has the sign of A_n opposite to the other two due to $J > 0$ in Fig. 2(b). So the system forms

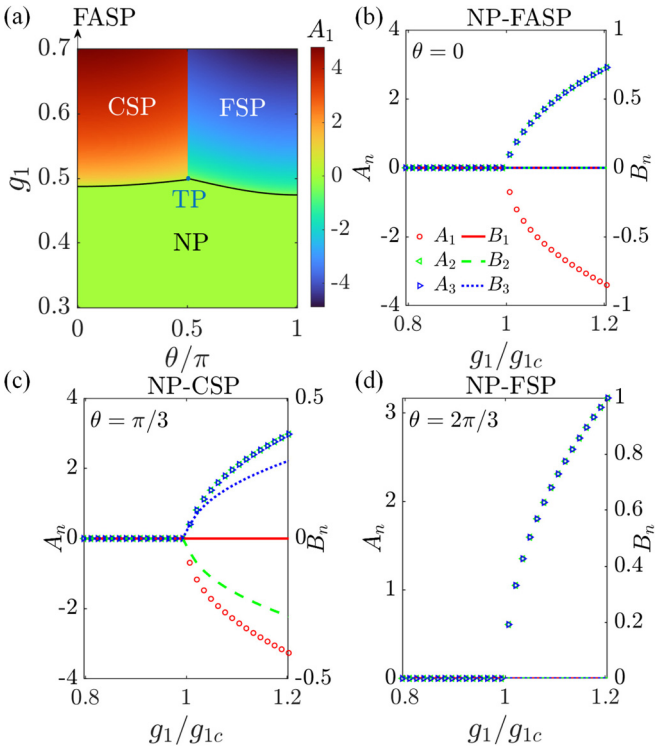

FIG. 2. (a) Phase diagram in the θ-g_1 plane for the quantum Rabi triangle. There occurs a phase transition from the NP to the FASP at $\theta = 0$. The critical line g_{1c} (solid black line) indicates the phase boundary from the NP to the CSP and the FSP by varying θ. The CSP, FSP, and NP join at the triple point (TP) at $\theta_c = 0.516\pi$. (b) The real part A_n and the imaginary part B_n of α_n as a function of g_1/g_{1c} at $\theta = 0$ for the NP-FASP transition. (c) A_n and B_n as a function of g_1/g_{1c} at $\theta = \pi/3 < \theta_c$ for the NP-CSP transition. (d) A_n and B_n as a function of g_1/g_{1c} at $\theta = 2\pi/3 > \theta_c$ for the NP-FSP transition.

a frustrated antiferromagnetic order, the so-called frustrated FASP. Second, for $0 < \theta < \theta_c$, it is in the CSP. Unlike the FASP, α_n of the frustrated cavity ($n = 1$) is real with the opposite sign, while it is complex for the remaining cavities in Fig. 2(c). It results in different mean photon numbers in the frustrated cavity. However, in the FSP with $\theta_c < \theta \leqslant \pi$, each cavity has the same mean photons with the same real value of α_n as in Fig. 2(d). It forms a ferromagnetic order with the same displacement of neighboring cavities due to the effective hopping strength $J\cos\theta < 0$ [27]. The critical value $g_{1c}^{\mathrm{CSP}}(q = -2\pi/3)$ in the CSP changes to $g_{1c}^{\mathrm{FSP}}(q = 0)$ in the FSP by varying the magnetic flux. It leads to the critical flux $\theta_c = \pm\cos^{-1}[-2J/(\sqrt{8J^2+\omega^2}+\omega)]$, which classifies the phase boundaries between the CSP and the FSP.

The Hamiltonian in Eq. (10) is bilinear in the creation and annihilation operators $\tilde{a}_n^\dagger$ and $\tilde{a}_n$. We perform a Bogoliubov transformation to diagonalize the Hamiltonian by using the bosonic operators $\beta = \{b_1^\dagger, b_2^\dagger, b_3^\dagger, b_1, b_2, b_3\}$, which are a linear combination of $\gamma = \{\tilde{a}_1, \tilde{a}_2, \tilde{a}_3, \tilde{a}_1^\dagger, \tilde{a}_2^\dagger, \tilde{a}_3^\dagger\}$. It satisfies $\gamma^\dagger = T\beta^\dagger$ with a paraunitary matrix T. To ensure the bosonic commutation relation, the paraunitary matrix T satisfies the relations of $T^\dagger\Lambda T = T\Lambda T^\dagger = \Lambda$, where $\Lambda = \begin{pmatrix} I_{3\times3} & 0 \\ 0 & -I_{3\times3} \end{pmatrix}$, with $I_{3\times3}$ being the identity matrix of order 3. Substituting for γ and $\gamma^\dagger$ in terms of $\beta^\dagger$ and β, one obtains the diagonalized form as $H_{\mathrm{eff}}^{\downarrow} = 2\sum_{k=1}^{3}\varepsilon_k b_k^\dagger b_k + (\varepsilon_k - \omega)/2$. The eigenvalues $\pm\varepsilon_k$ are obtained by diagonalizing the matrix ΛM as $T^{-1}\Lambda M T = \Lambda\varepsilon$ with the transformed Hamiltonian matrix M in Appendix A. The corresponding eigenvector gives the kth column vector of the paraunitary matrix as $T_k = [T_{1k}, T_{2k}, \ldots, T_{6k}]^T$.

The ground state of photons in the superradiant phases is the vacuum state

$$|\varphi_{\mathrm{SR}}\rangle = |0\rangle_{b_1}|0\rangle_{b_2}|0\rangle_{b_3}, \tag{13}$$

where $|0\rangle_{b_n}$ satisfies $b_n|0\rangle_{b_n} = 0$. Note that the operator b_n corresponds to the original operator a_n with the displacement transformation $D(\alpha)$ and the transformation T. It is straightforward to give $\tilde{a}_n = \sum_{i=1}^{3} T_{n,i}b_i + T_{n,i+3}b_i^\dagger + \alpha_n$. The local photon number in the nth cavity of the ground state $|\varphi_{\mathrm{SR}}\rangle$ is explicitly derived as

$$\langle a_n^\dagger a_n\rangle = |T_{n4}|^2 + |T_{n5}|^2 + |T_{n6}|^2 + |\alpha_n|^2. \tag{14}$$

The variances of x_n and p_n are obtained as

$$(\Delta x_n)^2 = |T_{n1} + T_{n4}^*|^2 + |T_{n2} + T_{n5}^*|^2 + |T_{n3} + T_{n6}^*|^2 \tag{15}$$

and $(\Delta p_n)^2 = |T_{n4}^* - T_{n1}|^2 + |T_{n5}^* - T_{n2}|^2 + |T_{n6}^* - T_{n3}|^2$, which are derived in detail in Appendix B. Thus, the quantum fluctuations of photons and the position variance are obtained beyond the mean-field approximation. We calculate the scaling behaviors of the critical fluctuations in the vicinity of the critical value g_c in the following.

IV. UNUSUAL CRITICAL EXPONENTS

Our major interests are the scaling exponents of quantum fluctuations as g_1 approaches g_{1c} for the second-order phase transitions from the NP to different superradiant phases. Generally, the energy gap measured by the lowest excitation energy ε_1 vanishes as g_1 approaches g_{1c}:

$$\varepsilon_1 \propto |g_1 - g_{1c}|^{\gamma}. \tag{16}$$

Here, the critical exponent $\gamma = z\nu$ is usually universal [6], which is independent of most of the parameters of the Hamiltonian. The variance of position quadrature diverges as

$$\Delta x \propto |g_1 - g_{1c}|^{-\nu} \tag{17}$$

with a critical exponent ν. Meanwhile, the fluctuations of the local mean photons near the critical value diverge as

$$\langle a_n^\dagger a_n\rangle \propto |g_1 - g_{1c}|^{-\beta}, \tag{18}$$

where β is a critical exponent. Using Bogoliubov's diagonalization method, we calculate the scaling exponents of the lowest excitation energy ε_1, the fluctuation of position variance $(\Delta x)^2$ in Eq. (15), and the mean photon number $\langle a_n^\dagger a_n\rangle$ in Eq. (14).

For the NP-FSP transition, the exponents of the excitation energy on the two sides of the phase transition are the same $\gamma = 1/2$ in Fig. 3(d), $\varepsilon_1 \propto |g_1 - g_{1c}|^{1/2}$, which is consistent with the analytical results of Eq. (7). And the mean photons of the nth cavity diverge as $\langle a_n^\dagger a_n\rangle \propto |g_1 - g_{1c}|^{-1/2}$ in Fig. 4(d). The fluctuation of Δx_n at the critical value gives the exponent $\nu = 1/4$ in Fig. 5(d), which diverges as $(\Delta x)_n^2 \propto$

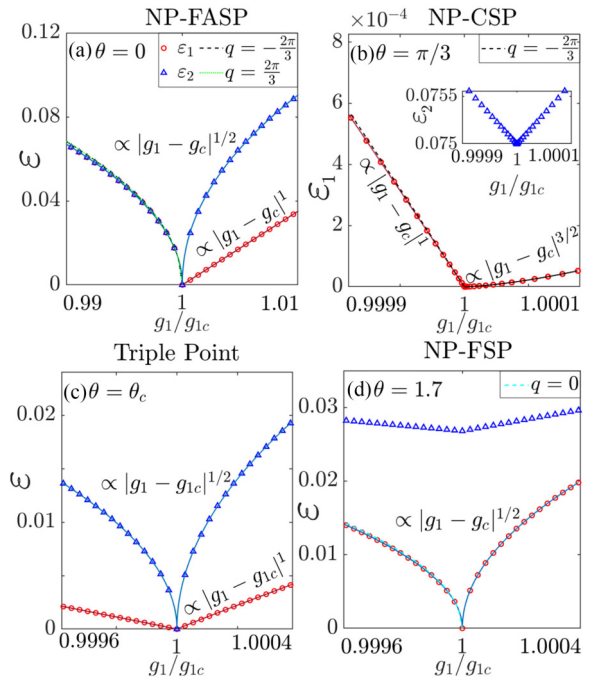

FIG. 3. The lowest excitation energy ε_1 and the second excitation energy ε_2 below and above the critical coupling strength g_{1c} for the NP-AFSP transition ($\theta = 0$) (a), the NP-CSR transition ($\theta = \pi/3 < \theta_c$) (b), the triple point ($\theta = \theta_c$) (c), and the NP-FSP transition ($\theta = 1.7 > \theta_c$) (d). The inset in panel (b) shows the second excitation energy ε_2 for the NP-CSP transition, which exhibits an obvious energy gap in comparison to ε_1. The analytical results of the lowest excitation energy in Eq. (3) are shown for $q = -2\pi/3$ (black dashed line), $q = 2\pi/3$ (solid green line), and $q = 0$ (blue dotted line) in panels (a), (b), and (d) for the NP ($g_1 < g_{1c}$).

$|g_1 - g_{1c}|^{-1/2}$. The exponent agrees well with the analytical one in Eqs. (8) and (9). The scaling exponents of the NP-FSP transition are the same as those of the conventional superradiant phase transition of the Rabi model [14,16] and the Dicke model [12,13]. The scaling laws hold with the same value of the exponent γ for both $g_1 > g_{1c}$ and $g < g_{1c}$.

For the NP-FASP transition with $\theta = 0$, Fig. 3(a) shows both the excitation energies ε_1 and ε_2 closing the gap at g_{1c} with the exponent $\gamma = 1/2$ for $g_1 < g_{1c}$. In contrast, for $g_1 > g_{1c}$, ε_1 and ε_2 vanish with different scaling behaviors:

$$\varepsilon_{1,\mathrm{FASP}} \propto (g_{1c} - g_1)^1, \quad \varepsilon_{2,\mathrm{FASP}} \propto (g_{1c} - g_1)^{1/2}. \tag{19}$$

It exhibits two different exponents γ_+ (γ_-) at the two sides of the phase transition for $g_1 > g_{1c}$ ($g < g_{1c}$), which is distinguished from conventional second-order phase transitions. Two different exponents $\gamma_+ = 1/2$ and $\gamma_+ = 1$ in Eq. (19) appear for $g_1 > g_{1c}$, for which the latter is the unconventional scaling exponent of the frustrated cavity $n = 1$. The distinct scaling behavior is consistent with results in the Dicke trimer [29]. Meanwhile, Fig. 4(a) shows the fluctuations of the mean photons in each cavity diverging with the same exponent $\beta_- = 1/2$ for $g_1 < g_{1c}$. However, for $g_1 > g_{1c}$, the photon number diverges locally dependent on n, which is associated with the frustrated geometry. $\langle a_n^\dagger a_n \rangle$ for the nth cavity exhibits

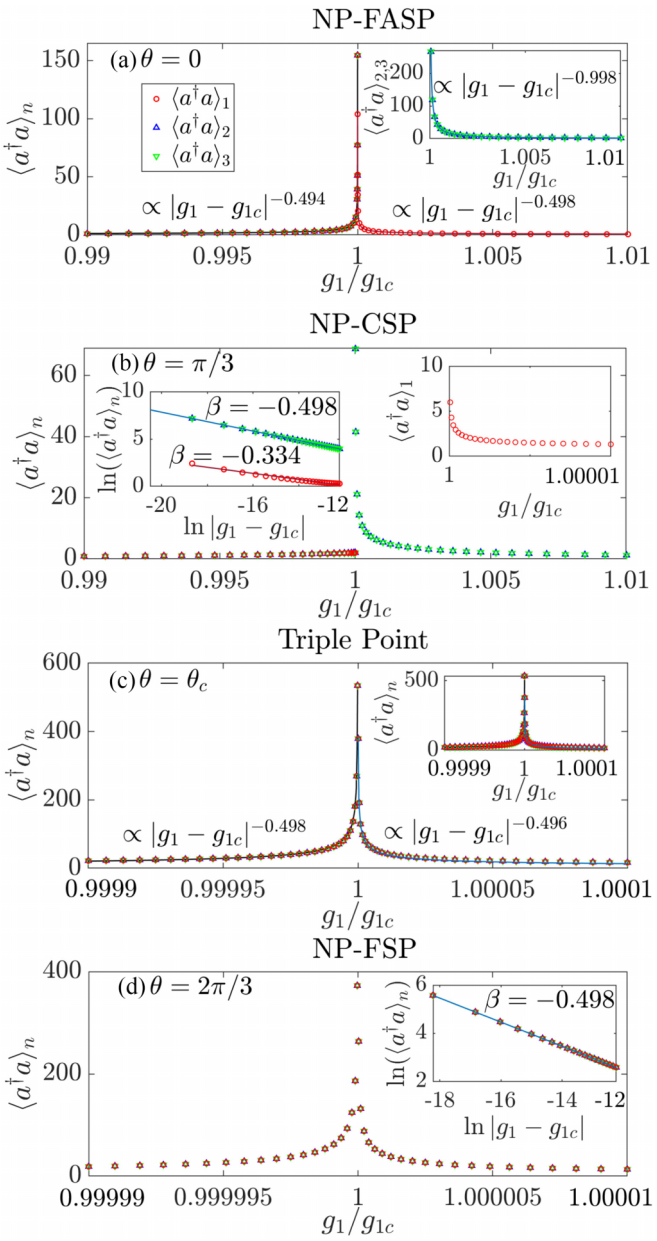

FIG. 4. Quantum fluctuations of the local mean photons for the nth cavity $\langle a_n^\dagger a_n \rangle$ as a function of g_1/g_{1c} for the NP-FASP transition ($\theta = 0$) (a), the NP-CSP transition ($\theta = \pi/3 < \theta_c$) (b), the triple point ($\theta = \theta_c$) (c), and the NP-FSP transition ($\theta = 2\pi/3 > \theta_c$) (d). The inset in panel (a) shows the scaling behavior of $\langle a_{2(3)}^\dagger a_{2(3)} \rangle$ [blue (green) triangles]. The right side of the inset in panel (b) shows the behavior of $\langle a_1^\dagger a_1 \rangle$ (red circles) in the frustrated cavity, and the left side shows the scaling exponents. The inset in panel (c) shows the scaling results by the solution in the CSP, which is same as the solution in the FSP. The inset in panel (d) shows the scaling exponent.

a different scaling law as follows:

$$\langle a_1^\dagger a_1 \rangle_{\mathrm{FASP}} \propto |g_1 - g_{1c}|^{-1},$$
$$\langle a_{2(3)}^\dagger a_{2(3)} \rangle_{\mathrm{FASP}} \propto |g_1 - g_{1c}|^{-1/2}. \tag{20}$$

The scaling of the frustrated cavity ($n = 1$) produces an unusual exponent $\beta = 1$, while the remaining cavities ($n = 2$ and 3) diverge with the same exponent $\beta = 1/2$ as in the Rabi

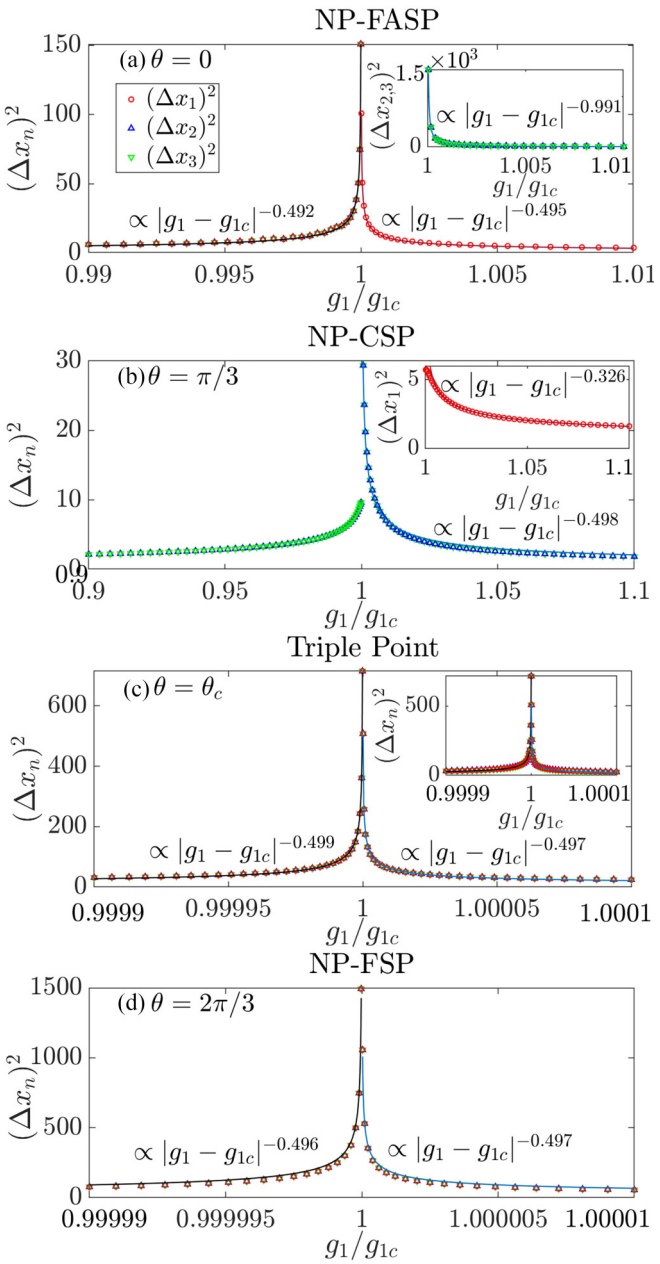

FIG. 5. Quantum fluctuation of the variance of position for the nth cavity $(\Delta x_n)^2$ as a function of g_1/g_{1c} for the NP-FASP transition ($\theta = 0$) (a), the NP-CSP transition ($\theta = \pi/3 < \theta_c$) (b), the triple point ($\theta = \theta_c$) (c), and the NP-FSP transition ($\theta = 2\pi/3 > \theta_c$) (d). The inset in panel (a) shows the scaling behavior of $(\Delta x_{2(3)})^2$. The inset in panel (b) shows the fluctuations of the first frustrated cavity $(\Delta x_1)^2$ above g_{1c}. The inset in panel (c) shows the scaling results by the solution in the CSP, which is the same as the solution in the FSP.

model, respectively. The similar n-dependent fluctuation of $(\Delta x_n)^2$ is shown in Fig. 5(a). The scaling exponent of Δx_n of each cavity below the critical value g_{1c} is the same $\nu_- = 1/4$ for $g_1 < g_{1c}$. By contrast, for $g_1 > g_{1c}$ the fluctuation diverges respectively as

$$(\Delta x_1)^2_{\mathrm{FASP}} \propto |g_1 - g_{1c}|^{-1},$$
$$(\Delta x_{2(3)})^2_{\mathrm{FASP}} \propto |g_1 - g_{1c}|^{-1/2}. \tag{21}$$

Thus, the scaling exponents for Δx_n are extracted as $\nu_+ = 1/2$ for the frustrated cavity ($n = 1$) and $\nu_+ = 1/4$ for the remaining cavities ($n = 2, 3$) when g_1 approaches the critical value from above.

For the NP-CSP transition with the artificial magnetic field ($0 < \theta < \theta_c$), the unusual mode ε_1 closes the gap for g_1 approaching g_{1c} from below or above in Fig. 3(b). It behaves as

$$\varepsilon_{1,\mathrm{NP}} \propto |g_1 - g_{1c}|, \quad \varepsilon_{1,\mathrm{CSP}} \propto |g_1 - g_{1c}|^{3/2}. \tag{22}$$

It gives two unconventional exponents $\gamma_- = 1$ and $\gamma_+ = 3/2$ below and above g_{1c}, which are different from the results in the NP-FASR transition. In contrast to the FASP, the artificial magnetic field induces the nontrivial chiral phase with the unusual critical exponent. Interestingly, nondivergent fluctuations of $\langle a_n^\dagger a_n\rangle_{\mathrm{NP}}$ and $(\Delta x_n)_{\mathrm{NP}}$ for $g_1 < g_{1c}$ are observed in Figs. 4(b) and 5(b). The numerical results are consistent with the analysis from Eqs. (5) and (6), which ascribe to the nonzero value of the denominator dependent on the momentum q. For $g_1 > g_{1c}$, the mean photon number on the frustrated cavity is different from the other two due to geometric frustration in Fig. 2(c). Figure 4(b) shows n-dependent scaling behaviors of the local photon number:

$$\langle a_1^\dagger a_1\rangle_{\mathrm{CSP}} \propto |g_1 - g_{1c}|^{-1/3},$$
$$\langle a_{2(3)}^\dagger a_{2(3)}\rangle_{\mathrm{CSP}} \propto |g_1 - g_{1c}|^{-1/2}. \tag{23}$$

$\langle a_1^\dagger a_1\rangle$ of the frustrated cavity diverges with the exponents $1/3$, which is different from that of the Dicke lattice [28]. Meanwhile, Fig. 5(b) shows the fluctuation of the position variance of the nth cavity, which diverges as

$$(\Delta x_1)^2_{\mathrm{CSP}} \propto |g_1 - g_{1c}|^{-1/3},$$
$$(\Delta x_{2(3)})^2_{\mathrm{CSP}} \propto |g_1 - g_{1c}|^{-1/2}. \tag{24}$$

The unusual exponent of the frustrated cavity ($n = 1$) $\nu_+ = 1/6$ for Δx_n is also different from $\nu_+ = 1/2$ in the FASP transition. It demonstrates that contributions from the geometry frustration and the artificial magnetic field lead to different unusual critical exponents. It exhibits distinct exponents of the frustrated cavity by comparing it to the NP-FASP transition without the magnetic flux.

At the triple point θ_c, there appear two excitation modes that close the gaps at g_{1c}. Figure 3(c) shows two different behaviors of power laws:

$$\varepsilon_{1,\mathrm{TP}} \propto |g_1 - g_{1c}|, \quad \varepsilon_{2,\mathrm{TP}} \propto |g_1 - g_{1c}|^{1/2}. \tag{25}$$

We obtain exponents $\gamma_\pm = 1$ and $\gamma_\pm = 1/2$. This is a signature of the coexistence of both the CSP and the FSP. And the scaling exponents are the same on the two sides of the TP. We calculate the fluctuation of $\langle a_n^\dagger a_n\rangle$ by the analytical solutions in the FSP phase in Fig. 4(c), which behaves the same as that in the CSR in the inset. Figure 5(c) shows the scaling laws of $(\Delta x_n)^2_{\mathrm{TP}}$. Thus, the scaling behaviors of the quantum fluctuations near the critical point can be expressed as

$$\langle a_n^\dagger a_n\rangle_{\mathrm{TP}} \propto |g_1 - g_{1c}|^{-1/2}, \quad (\Delta x_n)^2_{\mathrm{TP}} \propto |g_1 - g_{1c}|^{-1/2}. \tag{26}$$

Thus, we obtain the scaling exponents $\beta = 1/2$ and $\nu = 1/4$ at the triple point, respectively.

TABLE I. Scaling exponents $\gamma_\pm$ of the excitation energy ε_n, $\nu_\pm$, and $\beta_\pm$ for quantum fluctuations of the Δx_n and $\langle a_n^\dagger a_n\rangle$ on two sides of the phase transitions of the NP-FASP ($\theta = 0$), the NP-CSP ($\theta < \theta_c$), and the NP-FSP ($\theta > \theta_c$) as well as the triple point (TP) ($\theta = \theta_c$). Especially, the symbol "–" denotes that a particular exponent is nondivergent when g_1 approaches the critical value from below for the NP-CSP phase transition.

	γ_-	γ_+	ν_-	ν_+	β_-	β_+
NP-FASP	1/2	1, 1/2	1/4	1/2, 1/4	1/2	1, 1/2
NP-CSP	1	3/2	–	1/6, 1/4	–	1/3, 1/2
TP	1, 1/2	1, 1/2	1/4	1/4	1/2	1/2
NP-FSP	1/2	1/2	1/4	1/4	1/2	1/2

Various critical exponents for g_1 approaching g_{1c} from below and above are listed in Table I for different superradiant phase transitions. Scaling exponents below and above g_{1c} are different for the NP-FASP and NP-CSP transitions, while they are the same for the NP-FSP transition. In particular, for the NP-CSP phase transition, the exponents ν_- and β_- are nondivergent when g_1 approaches the critical value from below. For the special frustrated cavity, the unusual critical exponents of the photon fluctuations are $\beta_+ = 1$ and $\beta_+ = 1/3$ for the NP-FASP and NP-CSP transitions, respectively. Meanwhile, the anomalous exponents of the fluctuations in position variance are $\nu_+ = 1/2$ and $\nu_+ = 1/6$. They are distinguished from the exponents of the remaining cavities with $\beta_+ = 1/2$ and $\nu_+ = 1/4$. This reveals that the magnetic flux leads to unusual exponents compared to geometric frustrations, resulting in the distinct universality classes of the NP-CSP and NP-FASP transitions.

V. CONCLUSION

Quantum fluctuations and scaling behaviors in the Rabi triangle with an artificial magnetic field are investigated beyond the mean-field approximation. Our analytical method is an accurate solution even by involving the fluctuations terms and is valid for a large system of $N > 3$ under the constraints of a large frequency ratio of $\Delta/\omega \gg 1$ and a small hopping strength of $J/\omega \ll 1$. At the critical value, two scaling laws of the observables emerge, one for the frustrated cavity with an unusual exponent and the other for the remaining cavities with the same exponent as the conventional quantum Rabi model. It ascribes to the geometric frustrations of the triangular system. In addition, the frustrated cavity exhibits different scaling exponents by applying the magnetic flux in the chiral phase. Moreover, we find nondivergent quantum fluctuation below the critical value in the chiral phase, which is associated with the magnetic flux. The unconventional critical exponents predict different universality classes beyond the conventional superradiant phase transitions. Our work paves a way for exploring unconventional phase transitions in the few-body light-matter interacting systems.

ACKNOWLEDGMENTS

The authors thank Qing-Hu Chen and Xiang-You Chen for useful discussions. This work was supported by NSFC under Grants No. 12075040 and No. 12347101.

APPENDIX A: DIAGONALIZATION OF HAMILTONIAN IN THE SUPERRADIANT PHASE

After shifting the bosonic operator $\tilde{a}_n = a_n + \alpha_n$, the Hamiltonian in the superradiant phases becomes

$$H_{\rm SR} = \sum_{n=1}^{3} \omega \tilde{a}_n^\dagger a_n - \frac{\Delta_n}{2}\tau_n^z + \lambda_n(\tilde{a}_n^\dagger + \tilde{a}_n)\tau_n^x + J\tilde{a}_n^\dagger(e^{i\theta}\tilde{a}_{n+1} + e^{-i\theta}\tilde{a}_{n-1}) + V_{\rm off} + E_0, \tag{A1}$$

where the transformed Pauli matrix is $\tau_n^z = \Delta/\Delta_n\sigma_n^z + 4gA_n/\Delta_n\sigma_n^x$. The off-diagonal term is expressed as $V_{\rm off} = \sum_n \omega(\alpha_n\tilde{a}_n^\dagger + \alpha_n^*\tilde{a}_n) + g(\tilde{a}_n^\dagger + \tilde{a}_n)\sin(2\gamma_n)\sigma_n^z + J[\tilde{a}_n^\dagger(e^{i\theta}\alpha_{n+1} + e^{-i\theta}\alpha_{n-1}) + \text{H.c.}]$. By eliminating the $V_{\rm off}$ term, we obtain the equations explicitly of A_n and B_n in Eqs. (11) and (12). The Hamiltonian $H_{\rm SR}$ in Eq. (A1) has the same form as the original QRT Hamiltonian $H_{\rm QRT}$, one can obtain the effective Hamiltonian by using the similar Schrieffer-Wolff transformation described for the normal phase. Then we obtain the lowest-energy Hamiltonian in Eq. (10).

Using the denotation $\gamma = \{\tilde{a}_1, \tilde{a}_2, \tilde{a}_3, \tilde{a}_1^\dagger, \tilde{a}_2^\dagger, \tilde{a}_3^\dagger\}$, the Hamiltonian in Eq. (10) can be written in matrix form as $H_{\rm eff}^\downarrow = \gamma M \gamma^\dagger - 3(\omega - \lambda_n^2/\Delta_n)/2$, where a transformed matrix M is as follows:

$$M = \begin{pmatrix} \omega/2 - \lambda_1^2/\Delta_1 & Je^{-i\theta}/2 & Je^{i\theta}/2 & -\lambda_1^2/\Delta_1 & 0 & 0 \\ Je^{i\theta}/2 & \omega/2 - \lambda_2^2/\Delta_2 & Je^{-i\theta}/2 & 0 & -\lambda_2^2/\Delta_2 & 0 \\ Je^{-i\theta}/2 & Je^{i\theta}/2 & \omega/2 - \lambda_3^2/\Delta_3 & 0 & 0 & -\lambda_3^2/\Delta_3 \\ -\lambda_1^2/\Delta_1 & 0 & 0 & \omega/2 - \lambda_1^2/\Delta_1 & Je^{i\theta}/2 & Je^{-i\theta}/2 \\ 0 & -\lambda_2^2/\Delta_2 & 0 & Je^{-i\theta}/2 & \omega/2 - \lambda_2^2/\Delta_2 & Je^{i\theta}/2 \\ 0 & 0 & -\lambda_3^2/\Delta_3 & Je^{i\theta}/2 & Je^{-i\theta}/2 & \omega/2 - \lambda_3^2/\Delta_3 \end{pmatrix}. \tag{A2}$$

We perform a Bogoliubov transformation to give bosonic operators $\beta = \{b_1^\dagger, b_2^\dagger, b_3^\dagger, b_1, b_2, b_3\}$, which are a linear combination of $\gamma = \{\tilde{a}_1, \tilde{a}_2, \tilde{a}_3, \tilde{a}_1^\dagger, \tilde{a}_2^\dagger, \tilde{a}_3^\dagger\}$. It satisfies $\gamma^\dagger = T\beta^\dagger$ with a paraunitary matrix T. The Hamiltonian can be diagonalized as $H_{\rm eff}^\downarrow = \beta T^\dagger M T \beta^\dagger = 2\sum_{k=1}^3 \varepsilon_k b_k^\dagger b_k + (\varepsilon_k - \omega)/2$. The eigenvalues ε_k are obtained by diagonalizing the matrix ΛM, where $\Lambda = \left(\begin{smallmatrix} I_{3\times3} & 0 \\ 0 & -I_{3\times3} \end{smallmatrix}\right)$, with $I_{3\times3}$ being the identity matrix of order 3.

APPENDIX B: DERIVATIONS OF QUANTUM FLUCTUATIONS

In the superradiant phase, the operator a_n is shifted as $a_n + \alpha_n$. Using the Bogoliubov diagonalization method, the ground state of the photon part is obtained as $|\varphi_{\rm SR}\rangle = |0\rangle_{b_1}|0\rangle_{b_2}|0\rangle_{b_3}$, with $b_n|0\rangle_{b_n} = 0$. With the transformation $D(\alpha)$ and the transformation $\alpha^\dagger = T\beta^\dagger$, the operator a becomes $a_n = \sum_{i=1}^{3} T_{n,i}b_i + T_{n,i+3}b_i^\dagger + \alpha_n$. The expected value of $x_n = (a_n + a_n^\dagger)$ is given by

$$\begin{aligned}\langle x_n\rangle &= {}_{b_n}\langle 0|(a_n + a_n^\dagger)|0\rangle_{b_n}\\ &= \alpha_n + \alpha_n^* + {}_{b_n}\langle 0|\sum_{i=1}^{3} T_{n,i}b_i + T_{n,i+3}b_i^\dagger\\ &\quad + T_{n,i}^* b_i^\dagger + T_{n,i+3}^* b_i|0\rangle_{b_n}\\ &= \alpha_n^* + \alpha_n. \end{aligned} \tag{B1}$$

Then we derive the mean value of x_n^2 as

$$\begin{aligned}\langle x_n^2\rangle &= {}_{b_n}\langle 0|(a_n + a_n^\dagger + \alpha_n^* + \alpha_n)^2|0\rangle_{b_n}\\ &= \langle (a_n + a_n^\dagger)^2 + (\alpha_n^* + \alpha_n)(a_n + a_n^\dagger)\rangle + (\alpha_n^* + \alpha_n)^2\\ &= \langle\varphi_{\rm SR}|[(T_{n1} + T_{n4}^*)b_1 + (T_{n2} + T_{n5}^*)b_2\\ &\quad + (T_{n3} + T_{n6}^*)b_3 + \text{H.c.}]^2|\varphi_{\rm SR}\rangle + (\alpha_n^* + \alpha_n)^2\\ &= |T_{n1} + T_{n4}^*|^2 + |T_{n2} + T_{n5}^*|^2\\ &\quad + |T_{n3} + T_{n6}^*|^2 + (\alpha_n^* + \alpha_n)^2. \end{aligned}$$

The expected value of the variance of Δx_n is obtained as

$$\begin{aligned}(\Delta x_n)^2 &= \langle x_n^2\rangle - \langle x_n\rangle^2\\ &= |T_{n1} + T_{n4}^*|^2 + |T_{n2} + T_{n5}^*|^2 + |T_{n3} + T_{n6}^*|^2. \end{aligned} \tag{B2}$$

Additionally, the expected value of the momentum quadrature $p_n = i(a_n^\dagger - a_n)$ is

$$\langle p_n\rangle = {}_{b_n}\langle 0|i(a_n^\dagger - a_n + \alpha_n^* - \alpha_n)|0\rangle_{b_n} = i(\alpha_n^* - \alpha_n). \tag{B3}$$

The expected value of p_n^2 is derived as

$$\begin{aligned}\langle p_n^2\rangle &= {}_{b_n}\langle 0| - (a_n^\dagger - a_n + \alpha_n^* - \alpha_n)^2|0\rangle_{b_n}\\ &= -\langle (a_n^\dagger - a_n)^2 + (\alpha_n^* - \alpha_n)(a_n^\dagger - a_n)\rangle - (\alpha_n^* - \alpha_n)^2\\ &= -\langle |[(T_{n4}^* - T_{n1})b_1 + (T_{n5}^* - T_{n2})b_2 + (T_{n6}^* - T_{n3})b_3\\ &\quad - (T_{n4} - T_{n1}^*)b_1^\dagger - (T_{n5} - T_{n2}^*)b_2^\dagger - (T_{n6} - T_{n3}^*)b_3^\dagger]^2\rangle\\ &\quad - (\alpha_n^* - \alpha_n)^2\\ &= |T_{n4}^* - T_{n1}|^2 + |T_{n5}^* - T_{n2}|^2 + |T_{n6}^* - T_{n3}|^2\\ &\quad - (\alpha_n^* - \alpha_n)^2. \end{aligned} \tag{B4}$$

Then one obtains the variance of Δp_n:

$$\begin{aligned}(\Delta p_n)^2 &= \langle p_n^2\rangle - \langle p_n\rangle^2\\ &= |T_{n4}^* - T_{n1}|^2 + |T_{n5}^* - T_{n2}|^2 + |T_{n6}^* - T_{n3}|^2. \end{aligned} \tag{B5}$$

[1] M. J. Hartmann, F. G. S. L. Brandão, and M. B. Plenio, Nat. Phys. **2**, 849 (2006).
[2] D. Rossini and R. Fazio, Phys. Rev. Lett. **99**, 186401 (2007).
[3] I. Carusotto, D. Gerace, H. E. Tureci, S. De Liberato, C. Ciuti, and A. Imamoğlu, Phys. Rev. Lett. **103**, 033601 (2009).
[4] M. Schiró, M. Bordyuh, B. Öztop, and H. E. Türeci, Phys. Rev. Lett. **109**, 053601 (2012).
[5] M. Vojta, Rep. Prog. Phys. **66**, 2069 (2003).
[6] S. Sachdev, *Quantum Phase Transitions*, 2nd ed. (Cambridge University, Cambridge, England, 2011).
[7] J. Cardy, *Scaling and Renormalization in Statistical Physics* (Cambridge University Press, Cambridge, 1996).
[8] S. L. Sondhi, S. M. Girvin, J. P. Carini, and D. Shahar, Rev. Mod. Phys. **69**, 315 (1997).
[9] R. H. Dicke, Phys. Rev. **93**, 99 (1954).
[10] C. Emary and T. Brandes, Phys. Rev. E **67**, 066203 (2003).
[11] K. Baumann, R. Mottl, F. Brennecke, and T. Esslinger, Phys. Rev. Lett. **107**, 140402 (2011).
[12] Q.-H. Chen, Y.-Y. Zhang, T. Liu, and K.-L. Wang, Phys. Rev. A **78**, 051801(R) (2008).
[13] T. Liu, Y.-Y. Zhang, Q.-H. Chen, and K.-L. Wang, Phys. Rev. A **80**, 023810 (2009).
[14] M.-J. Hwang, R. Puebla, and M. B. Plenio, Phys. Rev. Lett. **115**, 180404 (2015).
[15] S. Ashhab, Phys. Rev. A **87**, 013826 (2013).
[16] M. Liu, S. Chesi, Z.-J. Ying, X. Chen, H.-G. Luo, and H.-Q. Lin, Phys. Rev. Lett. **119**, 220601 (2017).
[17] X.-Y. Chen, Y.-Y. Zhang, L. Fu, and H. Zheng, Phys. Rev. A **101**, 033827 (2020).
[18] X. Chen, Z. Wu, M. Jiang, X.-Y. Lü, X. Peng, and J. Du, Nat. Commun. **12**, 6281 (2021).
[19] M. L. Cai *et al.*, Nat. Commun. **12**, 1126 (2021).
[20] J. Dalibard, F. Gerbier, G. Juzeliūnas, and P. Öhberg, Rev. Mod. Phys. **83**, 1523 (2011).
[21] H. Cai, J. Liu, J. Wu, Y. He, S.-Y. Zhu, J.-X. Zhang, and D.-W. Wang, Phys. Rev. Lett. **122**, 023601 (2019).
[22] Y. Li, H. Cai, D.-W. Wang, L. Li, J. Yuan, and W. Li, Phys. Rev. Lett. **124**, 140401 (2020).
[23] P. Roushan, C. Neill, A. Megrant, Y. Chen, R. Babbush, R. Barends, B. Campbell, Z. Chen, B. Chiaro, A. Dunsworth *et al.*, Nat. Phys. **13**, 146 (2017).
[24] A. L. C. Hayward, A. M. Martin, and A. D. Greentree, Phys. Rev. Lett. **108**, 223602 (2012).
[25] A. L. C. Hayward and A. M. Martin, Phys. Rev. A **93**, 023828 (2016).
[26] Y.-Y. Zhang, Z.-X. Hu, L. Fu, H.-G. Luo, H. Pu, and X.-F. Zhang, Phys. Rev. Lett. **127**, 063602 (2021).
[27] D. Fallas Padilla, H. Pu, G.-J. Cheng, and Y.-Y. Zhang, Phys. Rev. Lett. **129**, 183602 (2022).
[28] J. Zhao and M.-J. Hwang, Phys. Rev. Res. **5**, L042016 (2023).
[29] J. Zhao and M.-J. Hwang, Phys. Rev. Lett. **128**, 163601 (2022).